Defence Technology 20 (2023) 24–33

Contents lists available at ScienceDirect

Defence Technology

journal homepage: www.keaipublishing.com/en/journals/defence-technology

Mechanical stress and deformation analyses of pressurized cylindrical shells based on a higher-order modeling

S. Mannani [a], L. Collini [b], M. Arefi [a, *]

[a] Department of Solid Mechanic, Faculty of Mechanical Engineering, University of Kashan, Kashan, 87317-51167, Iran
[b] Department of Engineering and Architecture, University of Parma, Parco Area Delle Scienze 181/A, 43124, Parma, Italy

ARTICLE INFO

Article history:
Received 17 May 2022
Received in revised form
9 June 2022
Accepted 4 July 2022
Available online 13 July 2022

Keywords:
Principle of virtual work
Thickness-stretched and shear deformable model
Stress and strain analyses
Cylindrical pressure vessel

ABSTRACT

In this research, mechanical stress, static strain and deformation analyses of a cylindrical pressure vessel subjected to mechanical loads are presented. The kinematic relations are developed based on higher-order sinusoidal shear deformation theory. Thickness stretching formulation is accounted for more accurate analysis. The total transverse deflection is divided into bending, shear and thickness stretching parts in which the third term is responsible for change of deflection along the thickness direction. The axisymmetric formulations are derived through principle of virtual work. A parametric study is presented to investigate variation of stress and strain components along the thickness and longitudinal directions. To explore effect of thickness stretching model on the static results, a comparison between the present results with the available results of literature is presented. As an important output, effect of micro-scale parameter is studied on the static stress and strain distribution.

1. Introduction

Analysis of pressure vessels have great importance in the context of mechanical engineering because of their vast applications in various situations. The cylindrical shells are used in various industrial applications such as chemical reactors, weapon instruments and aerospace technologies. Analysis of pressure vessels are performed using the Newtonian and Lagrangian methods and also using the technical codes proposed by important associations [1]. The Newtonian methods are applied through plane elasticity theory and are mostly valid for long cylindrical shells. The Lagrangian methods based on principle of virtual work and Hamilton's principle are used for more generalized formulation of the cylindrical shells with variable thickness and short length cylinder with axial boundary conditions. There are some applications of cylindrical shells in the various situations subjected to combination of mechanical, thermal and electrical loads [1–6] A review on the recent works is presented to justify significance of this paper.

Lori Dehsaraji et al. [7] formulated a higher-order thickness stretched piezoelectric nanoshell through Eringen nonlocal elasticity theory and shear and normal deformation theory. Decomposition of radial displacement into bending, shear and thickness stretching portions was used for kinematic relations. Justification of the results was performed through comparison with some lower order theories and also 3D results. Rezaiee-Pajand et al. [8] employed a higher order element including seven parameters to study nonlinear analysis of various thickness shell of revolution. Thickness stretching was accounted based on the employed element through finite element formulation. Zhang et al. [9] developed an experimental study on the fracture analysis of bituminous coal. Qiu et al. [10] studied effect of thermal load on the mechanical behavior of cylindrical shell as an energy storage.

Accounting concurrent geometric nonlinearity and thickness stretched model was employed by Amabili [11] for large amplitude vibration analysis of a doubly curved shell where all in-plane and transverse nonlinear terms were included in the formulation. The third-order thickness stretching formulation was used for analysis of laminated shell. The results were compared with those higher-order and refined theories that ignored thickness stretching. Lori Dehsaraji et al. [12] developed a modified couple stress model for electroelastic vibration analysis of cylindrical micro and nano shell

* Corresponding author. Department of Solid Mechanic, Faculty of Mechanical Engineering, University of Kashan, Kashan, 87317-51167, Iran.
E-mail addresses: arefi@kashanu.ac.ir, arefi63@gmail.com (M. Arefi).
Peer review under responsibility of China Ordnance Society

https://doi.org/10.1016/j.dt.2022.07.003

subjected to electromechanical loading through Hamilton's principle and a thickness stretching modeling. Patel et al. [13] investigated dynamic responses of elliptical shell made from functionally graded materials through higher-order modeling considering thickness stretching. To satisfy field consistency and avoid shear as well as membrane locking, the finite element approach was used for formulation. Ganapathi et al. [14] extended higher-order shear deformation theory to dynamic responses of laminated thick cylindrical shell with application in modeling the variation of the in/out of plane displacement and sudden discontinuity in the slope. Finite element method and time integration technique were employed for numerical investigation of the problem. Simo et al. [15] extended shell theory including finite thickness stretch as well as initial variable thickness for analysis of the problems including finite membrane strains, contact, delamination and concentrated surface loads. The numerical results were presented to investigate influence of thickness stretch on the responses of thin shell. Static, dynamic and stability analyses of a composite laminated shell was studied by Zenkour and Fares [16] based on Hamilton–Reissner's mixed variational principle. Polit et al. [17] studied effect of graphene nanoplatelets reinforcement and porosity on the static and stability analyses of curved beam based on higher-order model considering thickness stretching terms. Hamilton's principle and Navier's technique were employed for derivation of motion equations and solution procedure. Effect of thermal and fatigue loading was studied on the structural behavior of new materials and structures [18,19].

Arefi et al. [20] employed two-variable sinusoidal shear deformation theory for static bending analysis of a double curved shell with accounting shear and normal deformation theory. Generalized Hooke's law was used to derive governing equations. After derivation of the governing equations using principle of virtual work and solution using the analytical method, it was shown that accounting thickness stretching leads to a 4% improvement in the results. Amabili et al. [21] developed a new nonlinear model for nonlinear vibration characteristics of a shell made from hyperelastic material with incompressibility including nine parameters. The model was applicable for analysis of a Neo-Hookean material and biomechanics of soft tissues. Capability of the proposed model was justified through comparison of the results with those results without thickness stretching. Amabili [22] studied nonlinear forced vibration analysis of laminated cylindrical shell using the new higher-order shear deformation theory and Lagrange equations in which a harmonic point excitation along the radial direction was applied. Pseudo-arclength continuation method and bifurcation analysis were used to derive governing equations of motion. The accuracy of the proposed formulation was justified using reduction of the formulation to von Kármán formulation and Novozhilov theory. Chu [23] studied large amplitude vibration analysis of thin shell using a higher order shear deformable model and considering nonlinear strain components. Merodioand Haughton [24] studied bifurcation analysis of thick-walled cylindrical shell subjected to Marfan's syndrome. Bert and Birman [25] studied dynamic instability analysis of a cylindrical shell subjected to axial excitation made from orthotropic material reinforced with different fibers. Alsubari et al. [26] studied effect of humidity and thermal loads on the static analysis of anisotropic shell using generalized plane strain assumption and the Murakami zigzag function. There are some important works for referring the basic relations of this work [27–33,47–66].

Ganapathi et al. [34] used a new higher-order displacement field for dynamic responses of a thick multi-layered shell subjected to thermal and mechanical loads. Kumar et al. [35] employed a higher-order zigzag theory for finite element formulation of composite and sandwich shell. The failure criteria have been examined for the shell subjected to mechanical loadings. Ye et al. [36] combined a higher-order shear deformation theory and a semi-analytical method for formulation and numerical solution of a composite laminated shell using three-dimensional theory of elasticity. Shariyat and Eslami [37] studied dynamic buckling and postbuckling analyses of imperfect cylindrical shell in thermal environment using 3D thermoelasticity relations. Loy and Lam [38] presented higher-order dynamic formulation of a thick cylindrical shell based on elastodynamic relations. Third-order shear deformation theory was used in the framework of motion equations for free vibration responses of a cylindrical shell by Saad et al. [39]. The accuracy of the results was confirmed through comparison with finite element results. Desai and Kant [40] studied effect of sinusoidal higher order shear deformation theory on the bending behaviours of the cylindrical shell. Wavelet transform was used as a mathematical method for analysis of the engineering processes and applications [41–43]. For better and more accurate modeling the shear strains along the thickness direction, Bhimaraddi [44] used lower and higher order shear deformation theories for dynamic analysis of the cylindrical shells. McDaniel and Ginsberg [45] concurrently accounted higher-order shear deformation theory and Ritz expansions for vibration responses of the cylindrical shells. Hirano and Hirashima [46] used infinite power series along the radial direction for three dimensional dynamic analysis of a cylindrical shell based on a higher-order model. There are some applications [47–53] of new materials and technologies in the mechanical engineering such as reinforced materials.

Investigating related works on the recent published papers of cylindrical shells in various environments and using various theoretical formulation and kinetic relations has been performed in the literature survey. It is deduced that stress and deformation analysis of higher-order shear deformable cylindrical pressure vessels are important for more accurate analysis of the shells and should be accounted in new works. The importance of shear stress is confirmed in this paper specially at both ends. Two-variable sinusoidal shear deformation theory is used for description of kinematic relations and the principle of virtual work is used for derivation of the governing equations of motion.

2. Thickness stretching included formulation

An axisymmetric pressurized cylindrical pressure vessel is formulated in this section based on higher-order sinusoidal shear deformation theory and accounting thickness stretching. Based on the axisymmetric model, two axial u_x and radial w_z displacements are assumed in the framework of higher-order shear deformation theory accounting thickness stretching term are assumed as [65,66].

$$\begin{aligned} u_x &= u_0 - z\frac{\partial w_b}{\partial x} - f(z)\frac{\partial w_s}{\partial x} \\ w_z &= w_b + w_s + g(z)\chi \end{aligned} \tag{1}$$

in which, $f(z) = z - h/\pi \sin(\pi z/h)$ and $g(z) = 1 - f'(z)$. Furthermore, w_b, w_s, χ are bending, shear and stretching parts of

transverse deflection, respectively. Using the kinematic relations in the cylindrical coordinate system, the strain components are derived as [65,66].

$$\begin{aligned}
\varepsilon_{xx} &= \frac{\partial u_x}{\partial x} = \frac{\partial u_0}{\partial x} - z\frac{\partial^2 w_b}{\partial x^2} - f(z)\frac{\partial^2 w_s}{\partial x^2} \\
\varepsilon_{\theta\theta} &= \frac{w_z}{r} = \frac{w_b}{r} + \frac{w_s}{r} + \frac{g(z)}{r}\chi \\
\varepsilon_{zz} &= \frac{\partial w_z}{\partial z} = g'(z)\chi \\
\gamma_{xz} &= \frac{\partial u_x}{\partial z} + \frac{\partial w_z}{\partial x} = \{1 - f'(z)\}\frac{\partial w_s}{\partial x} + g(z)\frac{\partial \chi}{\partial x}
\end{aligned} \tag{2}$$

The behavioural relations are derived as [7,9,12]

$$\begin{Bmatrix} \sigma_{xx} \\ \sigma_{\theta\theta} \\ \sigma_{zz} \\ \tau_{xz} \end{Bmatrix} = \frac{E}{(1-2\vartheta)(1+\vartheta)} \begin{bmatrix} 1-\vartheta & \vartheta & \vartheta & 0 \\ \vartheta & 1-\vartheta & \vartheta & 0 \\ \vartheta & \vartheta & 1-\vartheta & 0 \\ 0 & 0 & 0 & \dfrac{1-2\vartheta}{2} \end{bmatrix} \times \begin{Bmatrix} \varepsilon_{xx} \\ \varepsilon_{\theta\theta} \\ \varepsilon_{zz} \\ \gamma_{xz} \end{Bmatrix} \tag{3}$$

where, normal (shear) stress and strain components are denoted with $\sigma_{ij}(\tau_{xz})$ and $\varepsilon_{ij}(\gamma_{ij})$. Furthermore, E, ϑ are Young's modulus and Poisson's ratio, respectively.

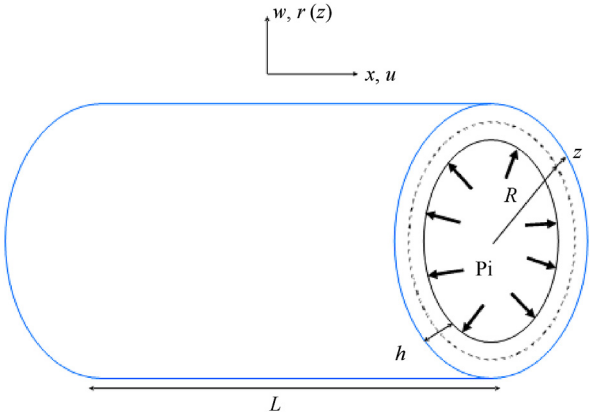

Strain energy variation of a cylindrical shell is expressed as [26–30,61,62,67].

$$\begin{aligned}
\delta U = \int_{x_1}^{x_2}\int_{z}\Bigg[& \sigma_{xx}\left(\frac{\partial\delta u_0}{\partial x} - z\frac{\partial^2\delta w_b}{\partial x^2} - f(z)\frac{\partial^2\delta w_s}{\partial x^2}\right) \\
& + \sigma_{\theta\theta}\left(\frac{\delta w_b}{r} + \frac{\delta w_s}{r} + \frac{g(z)}{r}\delta\chi\right) + \sigma_{zz}g'(z)\delta\chi \\
& + \tau_{xz}\left(\{1 - f'(z)\}\frac{\partial\delta w_s}{\partial x} + g(z)\frac{\partial\delta\chi}{\partial x}\right)\Bigg] dV
\end{aligned} \tag{4}$$

Through definition of resultant components, we will have the strain energy in the updated form as

$$\begin{aligned}
\delta U = 2\pi\int\Bigg[& N_{xx}\frac{\partial\delta u_0}{\partial x} - M_{xx}\frac{\partial^2\delta w_b}{\partial x^2} - S_{xx}\frac{\partial^2\delta w_s}{\partial x^2} + N_{\theta\theta}\delta w_b + N_{\theta\theta}\delta w_s \\
& + S_{\theta\theta}\delta\chi + S_{zz}\delta\chi + N_{xz}\frac{\partial\delta w_s}{\partial x} + S_{xz}\frac{\partial\delta\chi}{\partial x}\Bigg] dx
\end{aligned} \tag{5}$$

where the resultant components are defined as [7,9,12,67]:

$$\begin{aligned}
\{N_{xz}, M_{xx}, S_{xx}\} &= \int_z r\sigma_{xx}\{1, z, f(z)\}dz, \{N_{\theta\theta}, S_{\theta\theta}\} \\
&= \int_z \sigma_{\theta\theta}\{1, g(z)\}dz, S_{zz} = \int_z \sigma_{zz} r g(z) dz \\
\{N_{xz}, S_{xz}\} &= \int_z r\tau_{xy}\{\{1 - f'(z)\}, g(z)\}dz
\end{aligned} \tag{6}$$

Integration by part leads to

$$\begin{aligned}
\delta U = 2\pi\int\Bigg[& -\frac{\partial N_{xx}}{\partial x}\delta u_0 + \left(-\frac{\partial^2 M_{xx}}{\partial x^2} + N_{\theta\theta}\right)\delta w_b + \\
& \left(-\frac{\partial^2 S_{xx}}{\partial x^2} - \frac{\partial N_{xz}}{\partial x} + N_{\theta\theta}\right)\delta w_s + \left(S_{\theta\theta} + S_{zz} - \frac{\partial S_{xz}}{\partial x}\right)\delta\chi\Bigg] dx
\end{aligned} \tag{7}$$

The resultant components are defined in terms of displacement functions as

$$\begin{aligned}
N_{xx} &= \wp_1\frac{\partial u_0}{\partial x} - \wp_2\frac{\partial^2 w_b}{\partial x^2} - \wp_3\frac{\partial^2 w_s}{\partial x^2} + \wp_4 w_b + \wp_4 w_s \\
&\quad + \wp_5\chi + \wp_6\chi \\
M_{xx} &= \wp_7\frac{\partial u_0}{\partial x} - \wp_8\frac{\partial^2 w_b}{\partial x^2} - \wp_9\frac{\partial^2 w_s}{\partial x^2} + \wp_{10} w_b + \wp_{10} w_s \\
&\quad + \wp_{11}\chi + \wp_{12}\chi \\
S_{xx} &= \wp_{13}\frac{\partial u_0}{\partial x} - \wp_{14}\frac{\partial^2 w_b}{\partial x^2} - \wp_{15}\frac{\partial^2 w_s}{\partial x^2} + \wp_{16} w_b + \wp_{16} w_s \\
&\quad + \wp_{17}\chi + \wp_{18}\chi \\
N_{\theta\theta} &= \wp_{19} w_b + \wp_{19} w_s + \wp_{20}\chi + \wp_{21}\frac{\partial u_0}{\partial x} - \wp_{22}\frac{\partial^2 w_b}{\partial x^2} \\
&\quad - \wp_{23}\frac{\partial^2 w_s}{\partial x^2} + \wp_{24}\chi \\
S_{\theta\theta} &= \wp_{25} w_b + \wp_{25} w_s + \wp_{26}\chi + \wp_{27}\frac{\partial u_0}{\partial x} - \wp_{28}\frac{\partial^2 w_b}{\partial x^2} \\
&\quad - \wp_{29}\frac{\partial^2 w_s}{\partial x^2} + \wp_{30}\chi \\
S_{zz} &= \wp_{31}\chi + \wp_{32} w_b + \wp_{32} w_s + \wp_{33}\chi + \wp_{34}\frac{\partial u_0}{\partial x} - \wp_{35}\frac{\partial^2 w_b}{\partial x^2} \\
&\quad - \wp_{36}\frac{\partial^2 w_s}{\partial x^2} \\
N_{xz} &= \wp_{37}\frac{\partial w_s}{\partial x} + \wp_{38}\frac{\partial\chi}{\partial x} \\
S_{xz} &= \wp_{39}\frac{\partial w_s}{\partial x} + \wp_{40}\frac{\partial\chi}{\partial x}
\end{aligned} \tag{8}$$

where the integration constants are computed in Appendix A.

The external work due to internal and external pressures and an outer Pasternak's foundation is computed as follows [34–36,40–42].

$$\delta W = 2\pi \int\int \left[P_i \delta w_{z=-\frac{h}{2}} - P_o \delta w_{z=+h/2} - F_f \delta w_{z=+h/2} \right] \mathrm{d}z\mathrm{d}x \tag{9}$$

Substitution of transverse displacement into above relations leads to

$$\delta W = 2\pi \int\int \left[\left(P_i - P_o - F_f \right) \delta w_b + \left(P_i - P_o - F_f \right) \delta w_s \right] \mathrm{d}z\mathrm{d}x \tag{10}$$

The governing equations are derived as

$$\begin{aligned}
&\delta u_0 : -\frac{\partial N_{xx}}{\partial x} = 0 \\
&\delta w_b : -\frac{\partial^2 M_{xx}}{\partial x^2} + N_{\theta\theta} = P_i - P_o - F_f \\
&\delta w_s : -\frac{\partial^2 S_{xx}}{\partial x^2} - \frac{\partial N_{xz}}{\partial x} + N_{\theta\theta} = P_i - P_o - F_f \\
&\delta \chi : S_{\theta\theta} + S_{zz} - \frac{\partial S_{xz}}{\partial x} = 0
\end{aligned} \tag{11}$$

Finally, the governing equations in terms of primary functions are developed as

$$\begin{aligned}
&\delta u_0 : -\wp_1 \frac{\partial^2 u_0}{\partial x^2} + \wp_2 \frac{\partial^3 w_b}{\partial x^3} - \wp_4 \frac{\partial w_b}{\partial x} + \wp_3 \frac{\partial^3 w_s}{\partial x^3} - \wp_4 \frac{\partial w_s}{\partial x} - (\wp_5 + \wp_6) \frac{\partial \chi}{\partial x} = 0 \\
&\delta w_b : -\wp_7 \frac{\partial^3 u_0}{\partial x^3} + \wp_{21} \frac{\partial u_0}{\partial x} + \wp_8 \frac{\partial^4 w_b}{\partial x^4} - (\wp_{10} + \wp_{22} + K_p) \frac{\partial^2 w_b}{\partial x^2} + (\wp_{19} + K_w) w_b + \wp_9 \frac{\partial^4 w_s}{\partial x^4} - (\wp_{10} + \wp_{23} + K_p) \frac{\partial^2 w_s}{\partial x^2} \\
&\quad + (\wp_{19} + K_w) w_s - (\wp_{11} + \wp_{12}) \frac{\partial^2 \chi}{\partial x^2} + (\wp_{20} + \wp_{24}) \chi = P_i - P_o \\
&\delta w_s : -\wp_{13} \frac{\partial^3 u_0}{\partial x^3} + \wp_{21} \frac{\partial u_0}{\partial x} + \wp_{14} \frac{\partial^4 w_b}{\partial x^4} - (\wp_{16} + \wp_{22} + K_p) \frac{\partial^2 w_b}{\partial x^2} + (K_w + \wp_{19}) w_b + \wp_{15} \frac{\partial^4 w_s}{\partial x^4} - (\wp_{16} + \wp_{23} + \wp_{37} + K_p) \frac{\partial^2 w_s}{\partial x^2} \\
&\quad + (K_w + \wp_{19}) w_s - (\wp_{17} + \wp_{18} + \wp_{38}) \frac{\partial^2 \chi}{\partial x^2} + (\wp_{20} + \wp_{24}) \chi = P_i - P_o \\
&\delta \chi : (\wp_{34} + \wp_{27}) \frac{\partial u_0}{\partial x} - (\wp_{28} + \wp_{35}) \frac{\partial^2 w_b}{\partial x^2} + (\wp_{25} + \wp_{32}) w_b - (\wp_{29} + \wp_{36} + \wp_{39}) \frac{\partial^2 w_s}{\partial x^2} + (\wp_{25} + \wp_{32}) w_s - \wp_{40} \frac{\partial^2 \chi}{\partial x^2} \\
&\quad + (\wp_{26} + \wp_{30} + \wp_{31} + \wp_{33}) \chi = 0
\end{aligned} \tag{12}$$

3. Numerical results

Numerical solution procedure is explained in this section for simply-supported boundary conditions. The solution of governing equations is expressed based on trigonometric functions as

Table 1
Comparison between the dimensionless transverse deflection $\overline{w}$ between present results and those results of Refs. [31–33].

$S = R/h$	Soedel [32]	Khdeir et al. [33]	Nwojia and Ani [31]	Present
100	0.0019	0.0019	0.0019	0.00195
20	0.0206	0.0212	0.0214	0.0215
10	0.0301	0.0334	0.034	0.0342
4	0.0629	0.0616	0.0629	0.0632

$$\begin{Bmatrix} u_0 \\ w_b \\ w_s \\ \chi \end{Bmatrix} = \sum_n \sum_m \begin{Bmatrix} U\cos(\lambda_m x) \\ W_b \sin(\lambda_m x) \\ W \sin(\lambda_m x) \\ X \sin(\lambda_m x) \end{Bmatrix} \tag{13}$$

in which $\lambda_m = \frac{m\pi}{L}$. Two dimensional results including stresses, strains and displacements are explored along the radial and axial directions.

A validation through comparison of the present results with those results available in literature is presented. Listed in Table 1 is comparison between the dimensionless transverse deflection of the present results and those results of Refs. [31–33]. A good agreement between present results with literature results is observed.

The results including displacements, strains and stresses components are plotted along the axial and axial and radial directions. The results are presented for two different geometries of cylindrical shell. The first case is a long cylindrical shell: $R = 1$ m, $L = 5$ m, $t = 0.05$ m and the second case is a short cylindrical shell: $R = 1$ m, $L = 2$ m, $t = 0.1$ m.

Axial displacement is shown in Fig. 1 along the radial and axial directions for a pressurized cylindrical pressure vessel. The results of Fig. 1(a) and Fig. 1(b) are presented for $R = 1$ m, $L = 5$ m, $t = 0.02$ m and $R = 1$ m, $L = 2$ m, $t = 0.1$ m respectively. It is observed

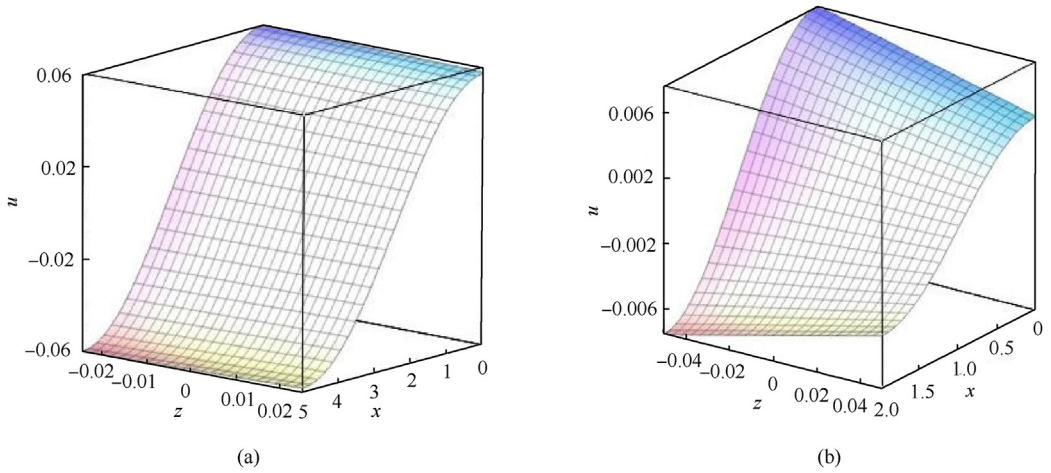

Fig. 1. Changes of axial displacement u along the radial and axial directions: (a) $R = 1$ m, $L = 5$ m, $t = 0.05$ m; (b) $R = 1$ m, $L = 2$ m, $t = 0.1$ m.

that for a long cylindrical pressure vessel, the axial displacement is approximately unchanged along the thickness direction. Unlike this case, the results of figure b are computed for a short and thick shell in which the radial displacement is changed along the thickness direction. It is confirmed that the higher-order shear deformation theory and thickness stretching leads to an efficient result for short and thick shells.

Shown in Fig. 2(a), Fig. 2(b) are two dimensional changes of radial displacements along the thickness and axial directions for cylindrical pressure vessel. The results are presented for two

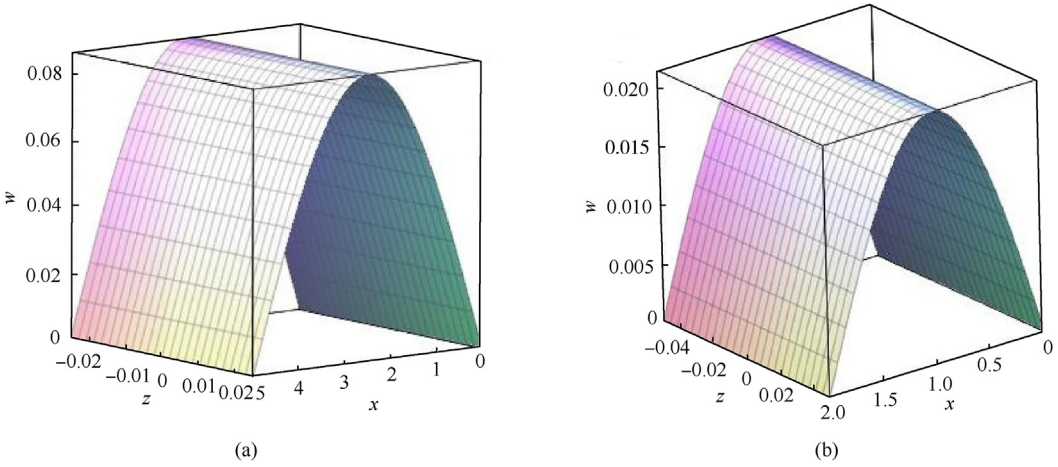

Fig. 2. Changes of transverse deflection w along the radial and axial directions: (a) $R = 1$ m, $L = 5$ m, $t = 0.05$ m; (b) $R = 1$ m, $L = 2$ m, $t = 0.1$ m.

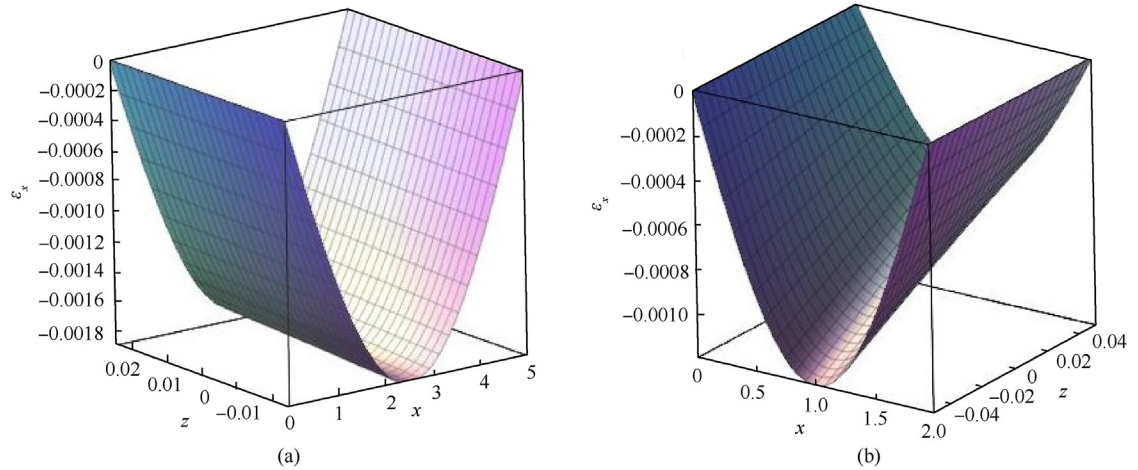

Fig. 3. Changes of axial strain ε_x along the radial and axial directions: (a) $R = 1$ m, $L = 5$ m, $t = 0.05$ m; (b) $R = 1$ m, $L = 2$ m, $t = 0.1$ m.

geometric cases. A significant decrease in the radial displacement is observed for a short length cylindrical shell $R = 1$ m, $L = 2$ m, $t = 0.1$ m respect to a long shell $R = 1$ m, $L = 5$ m, $t = 0.05$ m.

Two-dimensional variation of axial strain ε_x along the radial and axial directions is presented in Fig. 3(a), Fig. 3(b) for a pressurized cylindrical shell for two geometries. A decrease in axial strain ε_x is observed for a thick and short cylindrical shell. The maximum values of axial strain are observed at middle length of cylindrical shell due maximum bending moment at same section. Fig. 4, Fig. 5(a), Fig. 5(b) show two dimensional variation of radial ε_z and

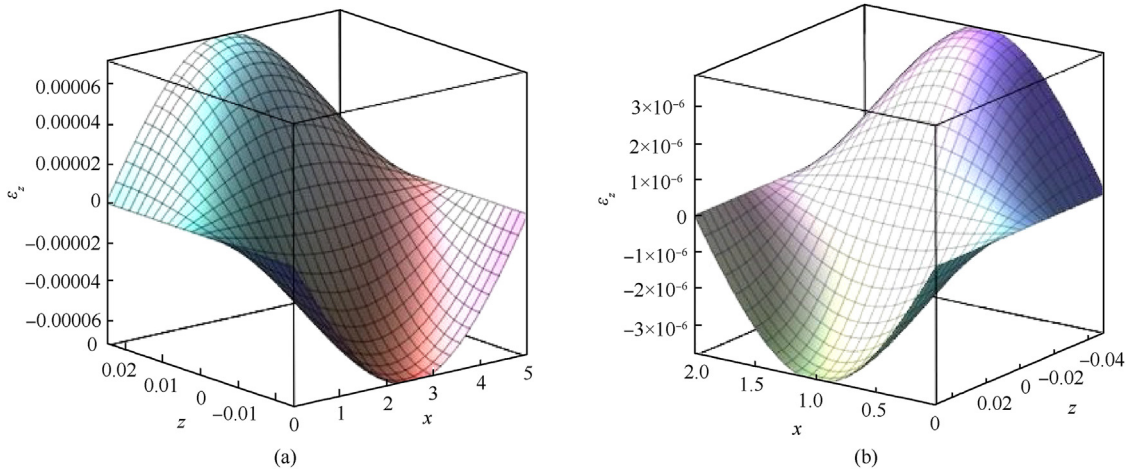

Fig. 4. Changes of radial strain ε_z along the radial and axial directions: (a) $R = 1$ m, $L = 5$ m, $t = 0.05$ m; (b) $R = 1$ m, $L = 2$ m, $t = 0.1$ m.

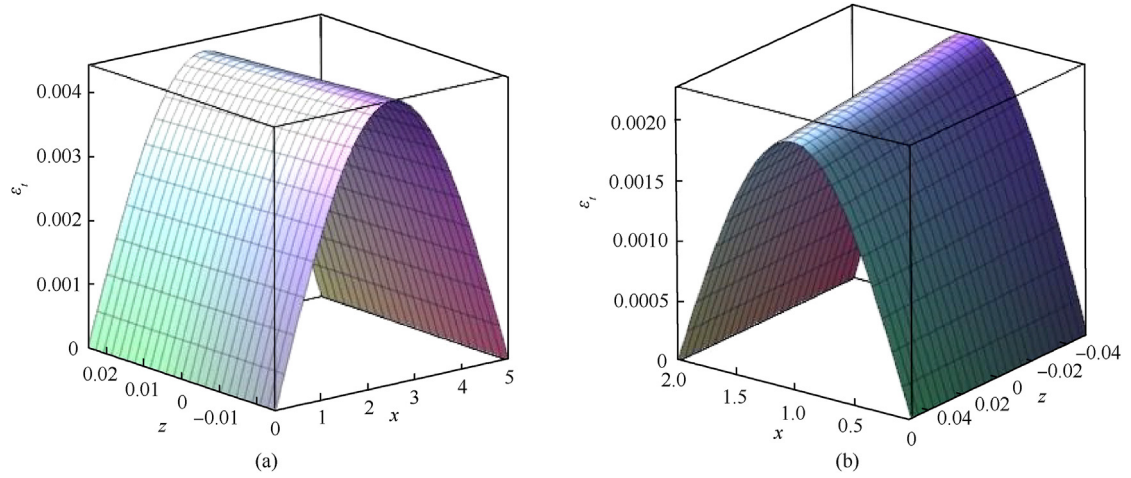

Fig. 5. Changes of hoop strain ε_t along the radial and axial directions: (a) $R = 1$ m, $L = 5$ m, $t = 0.05$ m; (b) $R = 1$ m, $L = 2$ m, $t = 0.1$ m.

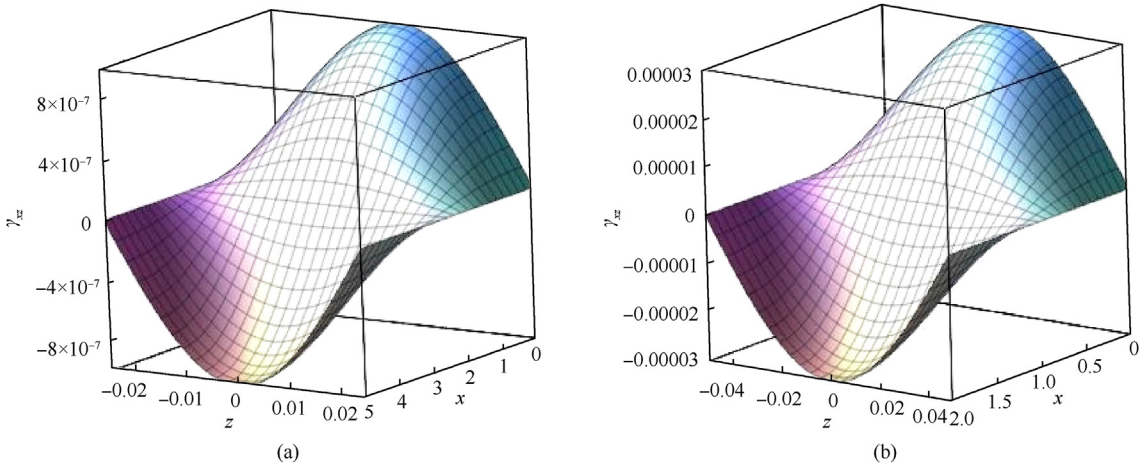

Fig. 6. Changes of shear strain γ_{xz} along the radial and axial directions: (a) $R = 1$ m, $L = 5$ m, $t = 0.05$ m; (b) $R = 1$ m, $L = 2$ m, $t = 0.1$ m.

circumferential ε_t strain components along the radial and axial directions. The results show that the radial strain is zero at both ends of cylindrical shell as well as middle surface.

Two dimensional variation of shear strain is presented in Fig. 6(a), Fig. 6(b) along the radial and axial directions. It is confirmed that the shear strain is zero at top and bottom surfaces. This condition has been justified using the proposed shear deformation theory.

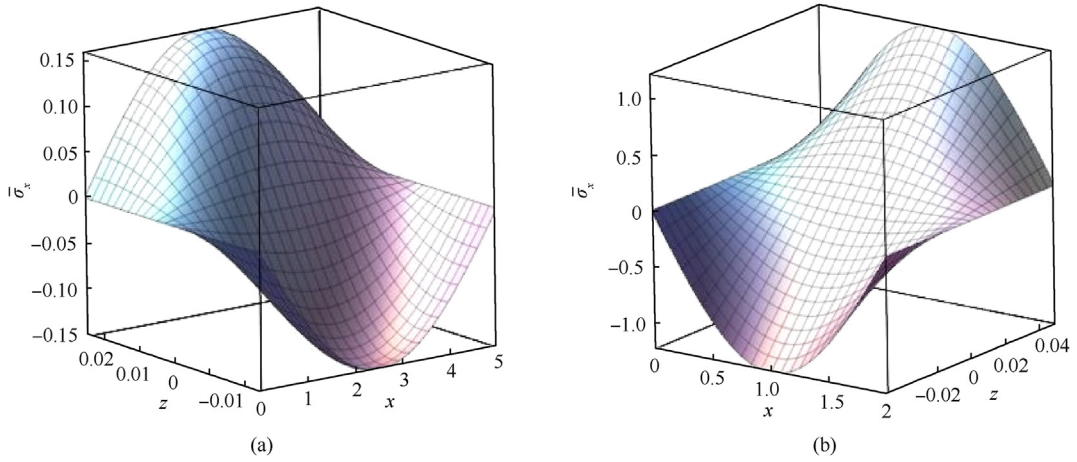

Fig. 7. Changes of non-dimensionless axial stress $\bar{\sigma}_x$ along the radial and axial directions: (a) $R = 1$ m, $L = 5$ m, $t = 0.05$ m; (b) $R = 1$ m, $L = 2$ m, $t = 0.1$ m.

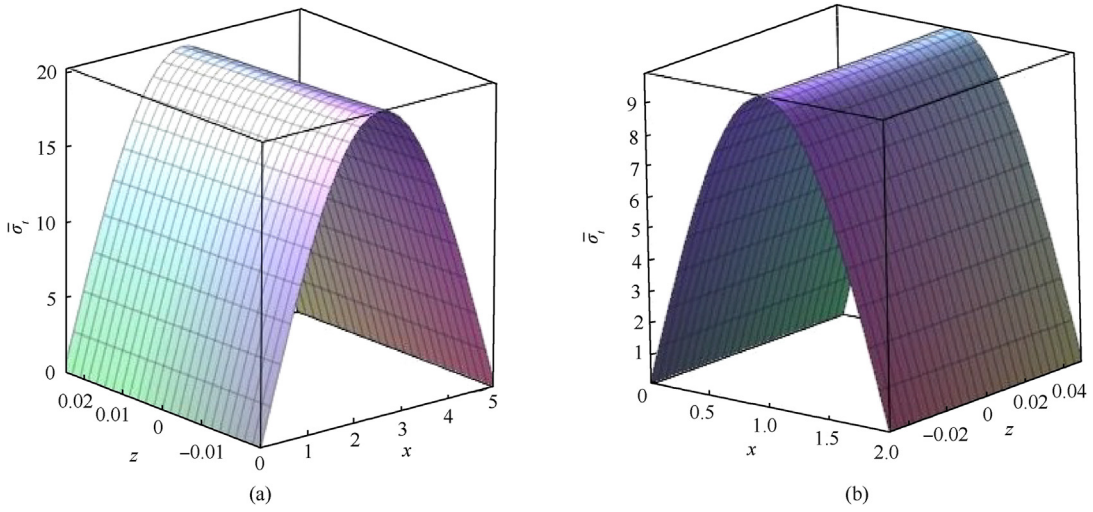

Fig. 8. Changes of non-dimensionless hoop stress $\bar{\sigma}_t$ along the radial and axial directions: (a) $R = 1$ m, $L = 5$ m, $t = 0.05$ m; (b) $R = 1$ m, $L = 2$ m, $t = 0.1$ m.

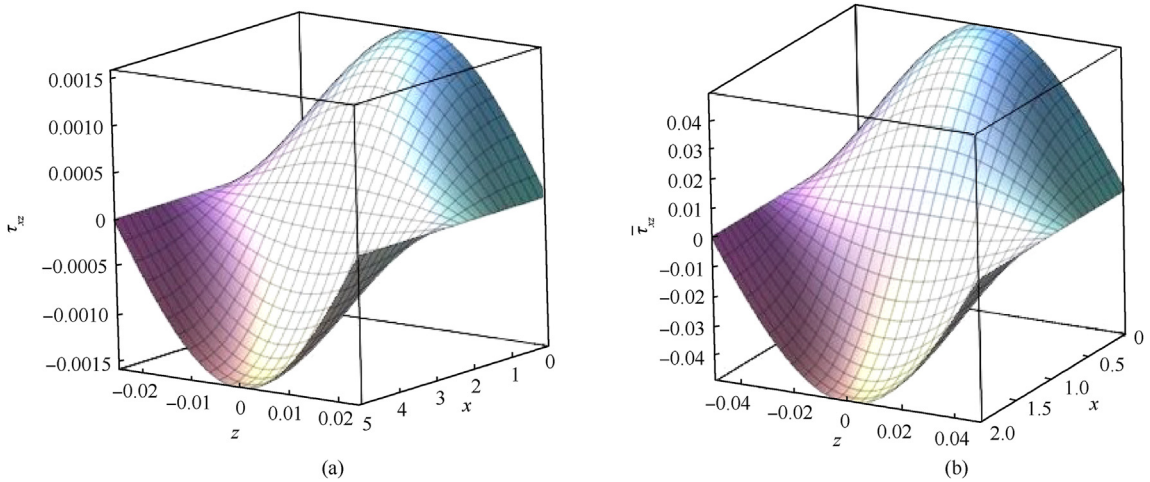

Fig. 9. Changes of non-dimensionless shear stress $\bar{\tau}_{xz}$ along the radial and axial directions: (a) $R = 1$ m, $L = 5$ m, $t = 0.05$ m; (b) $R = 1$ m, $L = 2$ m, $t = 0.1$ m.

Shown in Fig. 7(a), Fig. 7(b) are two dimensional variation of non-dimensional axial stress along the radial and axial directions. It is observed that the maximum stresses are occurred at the middle of the shell and the top and bottom surfaces. Existence of maximum normal stress at middle length of the shell is due to maximum bending moment at same section.

Shown in Fig. 8(a), Fig. 8(b) are changes of non-dimensional circumferential stress $\overline{\sigma}_t$ along the radial and axial directions for both long and short cylindrical shells. The maximum circumferential stress is occurred at the middle length of the shell where the maximum deflection is occurred. Small change of circumferential stress is observed along the thickness direction.

Shown in Fig. 9(a), Fig. 9(b) are changes of non-dimensionless shear stress $\overline{\tau}_{xz}$ along the radial and axial directions for both long and short cylindrical shells. It is observed that the shear stress is zero at top and bottom surfaces. Furthermore, the maximum shear stress is occurred at the middle surface.

4. Conclusions

Higher-order shear deformable model and thickness stretching formulation are employed in this research for mechanical stress, strain and deformation analyses of a cylindrical pressure vessel subjected to mechanical loads resting on Pasternak's foundation. The transverse deflection of the shell is assumed as the combination of bending, shear and stretching functions, in which the last term is responsible for variation of deflection along the thickness direction. After derivation of the governing equations through the principle of virtual work, the analytical solution is developed for stress and strain analyses. The mechanical stress, strain and deformation are presented along the length and thickness directions for two long and short cylindrical shells. A sinusoidal shape function is used for exact and accurate modeling of the shear stress along the thickness direction. The main results of this paper are classified as follows:

- The changes of results along the thickness direction indicates that there is no significant changes for all stress and strain components except shear stress and strain the are changed significantly.
- The results show that the transverse shear stress and strains are satisfied zero stress conditions at top and bottom surfaces.
- The results indicate that the main stress is hoop stress that should be accounted in design procedure.
- Based on the outputs, it is concluded that the shear strain and stress become very important for short cylindrical shells.

Declaration of competing interest

The authors declare that they have no known competing financial interests or personal relationships that could have appeared to influence the work reported in this paper.

Appendix A

$$\{\wp_1, \wp_2, \wp_3\} = \int_z r\Xi(1-\vartheta)\{1, z, f(z)\}\mathrm{d}z, \{\wp_4, \wp_5\} = \int_z \Xi\vartheta\{1, g(z)\}\mathrm{d}z, \{\wp_6\} = \int_z r\Xi\vartheta g'(z)\mathrm{d}z$$

$$\{\wp_7, \wp_8, \wp_9\} = \int_z zr\Xi(1-\vartheta)\{1, z, f(z)\}\mathrm{d}z, \{\wp_{10}, \wp_{11}\} = \int_z z\Xi\vartheta\{1, g(z)\}\mathrm{d}z, \{\wp_{12}\} = \int_z zr\Xi\vartheta g'(z)\mathrm{d}z$$

$$\{\wp_{13}, \wp_{14}, \wp_{15}\} = \int_z f(z)r\Xi(1-\vartheta)\{1, z, f(z)\}\mathrm{d}z, \{\wp_{16}, \wp_{17}\} = \int_z f(z)\Xi\vartheta\{1, g(z)\}\mathrm{d}z, \{\wp_{18}\} = \int_z f(z)r\Xi\vartheta g'(z)\mathrm{d}z$$

$$\{\wp_{19}, \wp_{20}\} = \int_z \frac{\Xi(1-\vartheta)}{r}\{1, g(z)\}\mathrm{d}z, \{\wp_{21}, \wp_{22}, \wp_{23}\} = \int_z \Xi\vartheta\{1, z, f(z)\}\mathrm{d}z, \{\wp_{24}\} = \int_z \Xi\vartheta g'(z)\mathrm{d}z$$

$$\{\wp_{25}, \wp_{26}\} = \int_z \frac{\Xi(1-\vartheta)}{r}g(z)\{1, g(z)\}\mathrm{d}z, \{\wp_{27}, \wp_{28}, \wp_{29}\} = \int_z \Xi\vartheta g(z)\{1, g(z)\}\{1, z, f(z)\}\mathrm{d}z, \{\wp_{30}\} = \int_z \Xi\vartheta g(z)g'(z)\mathrm{d}z$$

$$\wp_{31} = \int_z rg'(z)\Xi(1-\vartheta)g'(z)\mathrm{d}z, \{\wp_{32}, \wp_{33}\} = \int_z g'(z)\Xi\vartheta\{1, g(z)\}\mathrm{d}z, \{\wp_{34}, \wp_{35}, \wp_{36}\} = \int_z rg'(z)\Xi\vartheta\{1, z, f(z)\}\mathrm{d}z$$

$$\{\wp_{37}, \wp_{38}\} = \int_z \Xi\frac{1-2\vartheta}{2}r\{1-f'(z)\}\{\{1-f'(z)\}, g(z)\}\mathrm{d}z$$

$$\{\wp_{39}, \wp_{40}\} = \int_z \Xi\frac{1-2\vartheta}{2}rg(z)\{\{1-f'(z)\}, g(z)\}\mathrm{d}z$$

Appendix B. Supplementary data

Supplementary data to this article can be found online at https://doi.org/10.1016/j.dt.2022.07.003.

References

[1] Niranjana SJ, Patel SV, Dubey AK. Design and analysis of vertical pressure vessel using ASME code and FEA technique. IOP Conf Ser Mater Sci Eng 2018;376:012135.
[2] Chen F, Jin Z, Wang E, et al. Relationship model between surface strain of concrete and expansion force of reinforcement rust. Sci Rep 2021;11:4208.
[3] Wang X, Yang Y, Yang R, Liu P. Experimental analysis of bearing capacity of basalt fiber reinforced concrete short columns under axial compression. Coatings 2022;12(5):654.
[4] Civalek Ö. An efficient method for free vibration analysis of rotating truncated conical shells. Int J Pres Ves Pip 2006;83(1):1–12.
[5] Huang H, Huang M, Zhang W, Yang S. Experimental study of predamaged columns strengthened by HPFL and BSP under combined load cases. Struct Infrastruct Eng 2020;17(9):1210–27.
[6] Civalek Ö. Geometrically nonlinear dynamic analysis of doubly curved isotropic shells resting on elastic foundation by a combination of harmonic differential quadrature-finite difference method. Int J Pres Ves Pip 2005;82(6):470–9.
[7] Lori Dehsaraji M, Arefi M, Loghman A. Three dimensional free vibration analysis of functionally graded nano cylindrical shell considering thickness stretching effect, Steel and Composite Structures, vol. 34; 2020. p. 657–70. 5.
[8] Rezaiee-Pajand M, Masoodi AR, Arabi E. On the shell thickness-stretching effects using seven-parameter triangular element. Eur J Computat Mech 2018;27(2):163–85.
[9] Zhang L, Huang M, Li M, Lu S, Yuan X, Li J. Experimental study on evolution of fracture network and permeability characteristics of bituminous coal under repeated mining effect. Nat Resour Res 2021;31(1):463–86.
[10] Qiu L, He L, Lu H, Liang D. Pumped hydropower storage potential and its contribution to hybrid renewable energy co-development: a case study in the Qinghai-Tibet Plateau. J Energy Storage 2022;51:104447. 2022.
[11] Amabili M. A non-linear higher-order thickness stretching and shear deformation theory for large-amplitude vibrations of laminated doubly curved shells. Int J Non Lin Mech 2014;58:57–75.
[12] Lori Dehsaraji M, Arefi M, Loghman A. Size dependent free vibration analysis of functionally graded piezoelectric micro/nano shell based on modified couple stress theory with considering thickness stretching effect. Def Technol 2021;17(1):119–34.
[13] Patel BP, Gupta SS, Loknath MS, Kadu CP. Free vibration analysis of functionally graded elliptical cylindrical shells using higher-order theory. Compos Struct 2005;69(3):259–70.
[14] Ganapathi M, Patel BP, Pawargi DS. Dynamic analysis of laminated cross-ply composite non-circular thick cylindrical shells using higher-order theory. Int J Solid Struct 2002;39(24):5945–62.
[15] Simo JC, Rifai MS, Fox DD. on a stress resultant geometrically exact shell model. Part IV: variable thickness shells with through-the-thickness stretching. Comput Methods Appl Mech Eng 1990;81(1):91–126.
[16] Zenkour AM, Fares ME. Bending, buckling and free vibration of non-homogeneous composite laminated cylindrical shells using a refined first-order theory. Compos B Eng 2001;32(3):237–47.
[17] Polit O, Anant C, Anirudh B, Ganapathi M. Functionally graded graphene reinforced porous nanocomposite curved beams: bending and elastic stability using a higher-order model with thickness stretch effect. Compos B Eng 2019;166:310–27.
[18] Bai B, Nie Q, Zhang Y, Wang X, Hu W. Cotransport of heavy metals and SiO2 particles at different temperatures by seepage. J Hydrol 2021;597:125771.
[19] Cheng H, Sun L, Wang Y, Chen X. Effects of actual loading waveforms on the fatigue behaviours of asphalt mixtures. Int J Fatig 2021;151:106386.
[20] Arefi M, Mohammad-Rezaei Bidgoli E, Civalek O. Bending response of FG composite doubly curved nanoshells with thickness stretching via higher-order sinusoidal shear theory. Mech Base Des Struct Mach 2020. https://doi.org/10.1080/15397734.2020.1777157.
[21] Amabili M, Breslavsky ID, Reddy JN. Nonlinear higher-order shell theory for incompressible biological hyperelastic materials. Comput Methods Appl Mech Eng 2019;346:841–61.
[22] Amabili M. Nonlinear vibrations of laminated circular cylindrical shells: comparison of different shell theories. Compos Struct 2011;94(1):207–20.
[23] Chu H-N. Influence of large amplitudes on flexural vibrations of a thin circular cylindrical shell. AIAA 2012. https://doi.org/10.2514/8.9113.
[24] Merodio J, Haughton DM. Bifurcation of thick-walled cylindrical shells and the mechanical response of arterial tissue affected by Marfan's syndrome. Mech Res Commun 2010;37(1):1–6.
[25] Bert CW, Birman V. Parametric instability of thick, orthotropic, circular cylindrical shells. Acta Mech 1988;71:61–76.
[26] Alsubari S, Mohamed Ali JS, Aminand Y. Hygrothermoelastic analysis of anisotropic cylindrical shells. Compos Struct 2015;131:151–9.
[27] Sofiyev AH, Kuruoglu N. Buckling analysis of shear deformable composite conical shells reinforced by CNTs subjected to combined loading on the two-parameter elastic foundation. Def Technol 2022;18(2):205–18.
[28] Rao L, Lin C, Zhang C, Arefi M. Free vibration analysis of a cylindrical micro-shell based on MCST. Alex Eng J 2022;61(8):6293–303.
[29] Ebrahimi F, Hafezi P, Dabbagh A. Buckling analysis of embedded graphene oxide powder-reinforced nanocomposite shells. Def Technol February 2021;17(Issue 1):226–33.
[30] Melaibari AM, Abo-bakr R, Mohamed SA, Eltaher MA. Static stability of higher order functionally graded beam under variable axial load. Alex Eng J 2020;59(3):1661–75.
[31] Nwojia, C. U. Ani, D. G. Second−order models for the bending analysis of thin and moderately thick circular cylindrical shells, Lat Am J Solid Struct 19 (3), 2022.
[32] Soedel W. Vibrations of shells and plates. New York): Marcel Dekker, Inc; 2004.
[33] Khdeir AA, Reddy JN, Frederick D. A study of bending, vibration and buckling of cross-ply circular cylindrical shells with various shell theories. Int J Eng Sci 1989;27(11):1337–51.
[34] Ganapathi M, Patel BP, Pawargi DS, Patel HG. Comparative dynamic studies of thick laminated composite shells based on higher-order theories. Struct Eng Mech 2002;13(6):695–711.
[35] Kumar A, Chakrabarti A, Bhargava P, Prakash V. Efficient failure analysis of laminated composites and sandwich cylindrical shells based on higher-order zigzag theory. J Aero Eng 2015;28(4).
[36] Ye W, Li Z, Liu J, et al. Higher order semi-analytical solution for bending of angle-ply composite laminated cylindrical shells based on three-dimensional theory of elasticity. Thin-Walled Struct 2019;145:106392.
[37] Shariyat M, Eslami MR. Dynamic buckling and post-buckling of imperfect orthotropic cylindrical shells under mechanical and thermal loads, Based on the three-dimensional theory of elasticity. J Appl Mech 1999;66(2):476–84.
[38] Loy CT, Lam KY. Vibration of thick cylindrical shell on the basis of three-dimensional theory of elasticity. J Sound Vib 1999;226(4):719–37.
[39] Nuwairan MSA, Javed S. Free vibration of composite cylindrical shells based on third-order shear deformation theory. J Math 2021:3792164.
[40] Desai P, Kant T. On numerical analysis of axisymmetric thick circular cylindrical shells based on higher order shell theories by segmentation method. J Sandw Struct Mater 2015;17(2):130–69.
[41] Qiao W, Li Z, Liu W, Liu E. Fastest-growing source prediction of US electricity production based on a novel hybrid model using wavelet transform. Int J Energy Res 2022;46(2):1766–88.
[42] Qiao W, Liu W, Liu E. A combination model based on wavelet transform for predicting the difference between monthly natural gas production and consumption of US. Energy 2021;235:121216.
[43] Qiao W, Wang Y, Zhang J, Tian W, Tian Y, Yang Q. An innovative coupled model in view of wavelet transform for predicting short-term PM10 concentration. J Environ Manag 2021;289:112438.
[44] Bhimaraddi A. A higher order theory for free vibration analysis of circular cylindrical shells. Int J Solid Struct 1984;20(7):623–30.
[45] McDaniel JG, Ginsberg JH. Thickness expansions for higher-order effects in vibrating cylindrical shells. J Appl Mech 1993;60(2):463–9.
[46] Hirano K, Hirashima K. Formulation and accuracy of the circular cylindrical shell theory due to higher order approximation. JSME Int J Ser 1, Solid Mech Strength Mater 1989;32(3):337–40.
[47] Liu M, Li C, Zhang Y, et al. Cryogenic minimum quantity lubrication machining: from mechanism to application. Front Mech Eng 2021;16(4):649–97.
[48] Wu X, Li C, Zhou Z, et al. Circulating purification of cutting fluid: an overview. Int J Adv Manuf Technol 2021;117(9):2565–600.
[49] Gao T, Zhang Y, Li C, et al. Grindability of carbon fiber reinforced polymer using CNT biological lubricant. Sci Rep 2021;11:22535.
[50] Yang M, Li C, Said Z, et al. Semiempirical heat flux model of hard-brittle bone material in ductile microgrinding. J Manuf Process 2021;71:501–14.
[51] Li H, Zhang Y, Li C, et al. Extreme pressure and antiwear additives for lubricant: academic insights and perspectives. Int J Adv Manuf Technol 2022;120:1–27. 2022.
[52] Li H, Zhang Y, Li C, et al. Cutting fluid corrosion inhibitors from inorganic to organic: progress and applications. Kor J Chem Eng 2022;39:1107–34. 2022.
[53] Zhang XP, Li CH, Zhang YB, et al. Lubricating property of MQL grinding of Al2O3/SiC mixed nanofluid with different particle sizes and microtopography analysis by cross-correlation. Precis Eng 2017;47:532–45.
[54] Ghasemi M, Zhang C, Khorshidi H, Sun L. Seismic performance assessment of steel frames with slack cable bracing systems. Eng Struct 2022;250:113437.
[55] Wei J, Xie Z, Zhang W, Luo X, Yang Y, Chen B. Experimental study on circular steel tube-confined reinforced UHPC columns under axial loading. Eng Struct 2021;230:111599.
[56] Zhang H, Liu Y, Deng Y. Temperature gradient modeling of a steel box-girder suspension bridge using Copulas probabilistic method and field monitoring. Adv Struct Eng 2021;24(5):947–61.
[57] Xiao G, Chen B, Li S, Zhuo X. Fatigue life analysis of aero-engine blades for abrasive belt grinding considering residual stress. Eng Fail Anal 2015;131:2022. 105846.
[58] Liu C, Zhao Y, Wang Y, Zhang T, Jia H. Hybrid dynamic modeling and analysis of high-speed thin-rimmed gears. ASME J Mech Des 2021;143(12):123401.
[59] Fan-xiu C, Yi-chen Z, Xin-ya G, Zu-quan J, En-dong W, Fei-peng Z, Xiao-yuan H. Non-uniform model of relationship between surface strain and rust expansion force of reinforced concrete. Sci Rep 2021;11. Article number:

8741.
[60] Xiao X, Bu G, Ou Z, Li Z. Nonlinear in-plane instability of the confined FGP arches with nanocomposites reinforcement under radially-directed uniform pressure. Eng Struct 2022;252:113670.
[61] Hao R, Lu Z, Ding H, Chen L. A nonlinear vibration isolator supported on a flexible plate: analysis and experiment. Nonlinear Dynam 2022;108(2):941–58.
[62] Cheng H, Liu L, Sun L. Bridging the gap between laboratory and field moduli of asphalt layer for pavement infrastructure design and assessment: a comprehensive loading frequency-based approach. Front Struct Civ Eng 2022;16:267–80.
[63] Zhang L, Huang M, Xue J, Li M, Li J. Repetitive mining stress and pore pressure effects on permeability and pore pressure sensitivity of bituminous coal. Nat Resour Res 2021;30(6):4457–76.
[64] Xu Y, Zhang H, Yang F, Tong L, Yang Y, Yan D, Wu Y. Experimental study on small power generation energy storage device based on pneumatic motor and compressed air. Energy Convers Manag 2021;234:113949.
[65] Arefi M, Bidgoli EMR, Dimitri R, Tornabene F. Free vibrations of functionally graded polymer composite nanoplates reinforced with graphene nanoplatelets. Aero Sci Technol 2018;81:108–17.
[66] Arefi M, Bidgoli EMR, Dimitri R, Bacciocchi M, Tornabene F. Application of sinusoidal shear deformation theory and physical neutral surface to analysis of functionally graded piezoelectric plate. Compos B Eng 2019;151:35–50.
[67] Ghabussi A, Ashrafi N, Shavalipour A, Hosseinpour A, Habibi M, Moayedi H, et al. Free vibration analysis of an electro-elastic GPLRC cylindrical shell surrounded by viscoelastic foundation using modified length-couple stress parameter. Mech Based Des Struct Mach 2021;49(5):738–62.